The Journal of Experimental Biology 210, 2819-2828
Published by The Company of Biologists 2007
doi:10.1242/jeb.004697

Behavioral evidence for within-eyelet resolution in twisted-winged insects (Strepsiptera)

Srdjan Maksimovic, John E. Layne and Elke K. Buschbeck*
Department of Biological Sciences, University of Cincinnati, Cincinnati, OH 45221-0006, USA
*Author for correspondence (e-mail: elke.buschbeck@uc.edu)

Accepted 12 May 2007

Summary

Compound eyes are typically composed of hundreds to thousands of ommatidia, each containing 8–10 receptors. The maximal spatial frequency at which a compound eye can sample the environment is determined by the inter-ommatidial angle. Males of the insect order Strepsiptera are different: their eyes are composed of a smaller number of relatively large units (eyelets), each with an extended retina. Building on a study of *Xenos vesparum*, we use a behavioral paradigm based on the optomotor response to investigate the possibility that the eyelets of the Strepsiptera *Xenos peckii* are image-forming units. From anatomical evidence, we hypothesize that spatial sampling in the strepsipteran eye is determined not only by the interactions of widely spaced photoreceptors in different eyelets, but also by the angular separation between groups of closely spaced photoreceptors within eyelets. We compared *X. peckii*'s optomotor response with the predictions of an elementary motion detector (EMD) model consisting of two distinctly different sampling bases. The best match between our empirical results and the model shows that the optomotor response in *X. peckii* males is determined by both the small (intra-eyelet) and large (possibly inter-eyelet) separations. Our results indicate that the *X. peckii* eye has sampling bases around 10° and 20°, and that each eyelet could be composed of up to 13 sampling points, which is consistent with previous anatomical findings. This study is the first to use the EMD model explicitly to investigate the possibility that strepsipteran eyes combine motion detection features from both camera and compound eyes.

Key words: insect, eye, optomotor response.

Introduction

Due to the diversity of insects and crustaceans, the most common types of eyes are compound eyes. Among insects there is one small group of 'odd' insects called Strepsiptera (twisted-wing insects) that have eyes that are fundamentally different from other compound eyes (Kinzelbach, 1967; Kinzelbach, 1971; Kritsky et al., 1977; MacCarthy, 1991; Wachmann, 1972; Buschbeck et al., 1999; Pix et al., 2000), and may represent an intermediate form between camera eyes and compound eyes. While compound eyes are usually composed of thousands of ommatidia, each of which effectively samples no more than one point in space (Nilsson, 1989), Strepsiptera have relatively few shallow, camera-type eyelets, each with an extensive underlying retina (Strohm, 1910; Rösch, 1913; Paulus, 1979). This unique arrangement raises the possibility that the animal can resolve multiple image points with each eyelet (Buschbeck et al., 1999; Buschbeck et al., 2003). In this study we use an approach similar to that of Pix et al., who studied *Xenos vesparum* (Pix et al., 2000), to assess the visual resolution of a closely related species, *X. peckii*. We compare our behavioral results to a motion detection model that allows sampling bases (the angular separation of input elements) to differ for elementary motion detectors (EMD) that are situated within eyelets, and those that are between eyelets. Our data and model suggests that image resolution within eyelets indeed is the case for the motion detection pathway, and that each eyelet resolves about 13 points.

The Strepsiptera are a peculiar parasitic insect order that differs in many ways from other insects (Proffitt, 2005). Extreme sexual dimorphism in some instances makes it impossible to fully describe the life cycle of some species. Their phylogenetic position remains unresolved, partly because molecular analyses are controversial as Strepsiptera have an unusually small genome (Johnston et al., 2004). *Xenos peckii*, a parasite of the paper wasp *Polistes fuscatus*, are in most places rare, even if hosts are abundant, though in some areas the infestation rates of *Polistes* wasps by *Xenos* can be up to 60% (Hughes et al., 2003). Adult males are slightly more than 3 mm long and unable to feed. Their mature life only lasts a few hours, during which they are devoted to finding a mate. Females remain within the wasp's body for their entire life, and only protrude through the wasp cuticle to mate with the male outside. Not surprisingly, only males have eyes, and on average each eye has only about 50 lenses, in contrast to the slightly smaller but much better known fly *Drosophila melanogaster*, which has around 700 facets per eye. The average lens in *X. peckii* is around 65 μm in diameter and covers about the same area as 15 *D. melanogaster* lenses (Buschbeck et al., 2003).

The difference between Strepsiptera and more typical insects

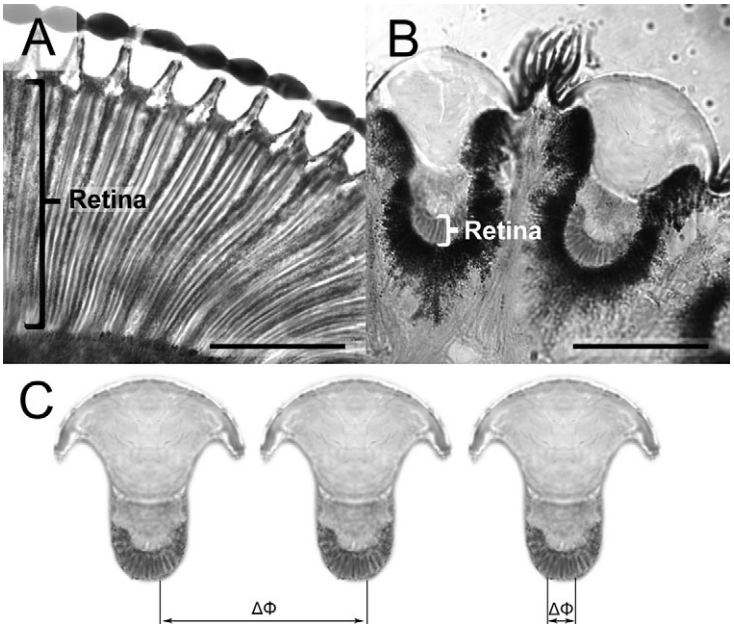

Fig. 1. Comparison of eye anatomy of *Drosophila melanogaster* (A) and *Xenos peckii* (B). The retina of *D. melanogaster* is composed of hundreds of long, narrow ommatidia, each containing eight receptor cells. In *X. peckii* an extended, cup-shaped retina lies beneath each of the large lenses. (C) Two principal sample bases (ΔΦ) are hypothesized: a smaller ΔΦ based on comparisons within eyelets (right), and a larger ΔΦ based on comparisons between photoreceptors in neighboring eyelets (left). Scale bars, 50 μm.

is even more pronounced in histological cross-sections of the eyes. While compound eyes like those of *Drosophila* are organized into a series of ommatidial units having a peripheral lens, crystalline cone, support cells and usually 8–10 receptor cells (Fig. 1A), cross-sections of *X. peckii* eyes show that beneath each biconvex lens lies a shallow, extended retina with more that 100 receptor cells (Fig. 1B) (Buschbeck et al., 2003). Pix et al. cleverly exploited the phenomenon of geometric interference to determine the spatial wavelength at which spatial aliasing caused a moving grating to reverse apparent direction (Pix et al., 2000). According to sampling theory this wavelength is equal to twice the effective sampling interval of the visual system. By modeling the optomotor behavior of *Xenos vesparum*, they showed that its eyes sampled the grating with a spatial interval corresponding to the angular separation between eyelets, casting doubt on the notion that points within an eyelet are processed for motion detection. Their modeling approach incorporated considerable variance around the mean sampling base (separation between input channels) in order to fit their empirical data, particularly the lack of a reversal of the response at small spatial wavelengths (Pix et al., 2000). Their assumption of variance is well supported by the highly irregular lens array of male Strepsiptera, and the inevitable variability in the way the vertical edges of the visual stimulus project onto the array of receptors.

In the current study we build upon the work of Pix et al. (Pix et al., 2000) by expanding their model, and making empirical measurements with *Xenos peckii*. Our motivations for repeating – with modifications – their study are the following:

(1) The anatomical organization of strepsipteran eyes suggests there could be two principal sampling bases: (a) the angular separation of clusters of receptor cells within eyelets and (b) potentially the separation of receptors in different eyelets (Fig. 1C). We expanded the model introduced by Pix et al. (Pix et al., 2000) to explicitly include these two disparate sampling bases (one small and one large) while maintaining the possibility for variation within each of them.

(2) Our study is on *Xenos peckii*, which has fewer and larger eyelets than *Xenos vesparum*. This should make it easer to detect within-eyelet resolution if it is present.

(3) In contrast to the behavioral response of *X. vesparum* (Pix et al., 2000), our preliminary studies on *X. peckii* found evidence for spatial aliasing. Therefore our behavioral results are more similar to those of other insects, and perhaps somewhat easier to interpret.

(4) Finally, because the shape of the behavioral response curve near the zero crossing is particularly critical, we tested these spatial wavelengths (between 15° and 24°) at finer intervals.

Detailed explanations of the optomotor response can be found elsewhere (e.g. Pix et al., 2000), so here we provide only a basic summary. The optomotor response is a stereotyped behavior comprising whole-body rotations that allow flying insects to maintain course by compensating for involuntary deviations from the original flight path (Srinivasan et al., 1999), or of head rotations that reduce rotational image velocity across the retina (Land, 1999). This response can be elicited with a patterned grating that is moved around a tethered insect. A left or rightward image shift across the retina causes the insect to make compensatory head movements in the same direction to minimize the relative motion between the eyes and visual scene. In order to explain the underlying mechanisms of this behavior, the phenomenological motion vision model known as the ‘correlation model’ has been developed and widely accepted. The simplest representation of this model that will signal motion in a directionally selective way has to have at least two input channels, the signals from which must be transmitted with different velocities or delays, and the subsequent interaction between which must be nonlinear (for reviews, see Borst and Egelhaaf, 1989; Borst and Egelhaaf, 1993; Egelhaaf and Borst, 1993). The network known as the ‘elementary motion detector’ (EMD) consists of two such subunits in mirror symmetry and sharing two input channels, and works on a delay-and-compare mechanism. The moving stimulus activates the two input channels in succession; in one subunit the signal from the first channel is delayed and then compared with the signal from the second channel in a multiplicative fashion (nonlinear interaction), while in the other subunit the second signal is delayed relative to the first. Subtracting the output signals of the subunits leads to a response that is directionally selective: the subunit in which the first channel is delayed relative to the second indicates the direction of the stimulus (at least relative to this two-point sample). EMD models of the correlation type have been used to explain motion detection in both invertebrates and vertebrates (Borst and Egelhaaf,

1989), and they allow the estimation of the parameters that determine the animal's response to moving stimuli such as moving patterned gratings. By adjusting the parameters so that the EMD model response matches the animal's optomotor response, one can determine the sampling base ($\Delta\phi$, angular separation) between input channels and acceptance angle ($\Delta\rho$) of input channels.

Materials and methods

Animals

During summer 2004 and 2005 *Polistes fuscatus* F infected with fertilized *Xenos peckii* females were collected in the vicinity of Cincinnati, OH, USA. A number of *Polistes fuscatus* nests were also collected and kept in the laboratory on honey, water and freshly killed crickets. As soon as the fertilized *X. peckii* females started producing first instar larvae, the *P. fuscatus* nests were manually infested with first instar parasites. Obtaining sufficient numbers of live Strepsiptera is difficult and time consuming, so this approach is necessary to get a sufficient number of *X. peckii* males. After a few weeks adult wasps carrying pupa of *X. peckii* males were separated from the rest of the wasps and frequently monitored for the emergence of adult *X. peckii* males. One challenge when working with male *X. peckii* is that, under laboratory conditions, they only live for 2–6 h. Therefore it is critical to start behavioral tests within 30 min of emergence. In order to be able to do so, late pupa were kept in the dark throughout the night and early morning of the final days of pupal development. Emergence of adults was triggered by exposure to bright light.

Histology and scanning electron microscopy (SEM)

Histological sections were prepared using a protocol by Strausfeld and Seyan (Strausfeld and Seyan, 1985) with a minor modification. Insects were anesthetized by chilling, decapitated, and part of the head cuticle removed. Heads were fixed in 4% paraformaldehyde solution (EM grade; Electron Microscopy Sciences, Fort Washington, PA, USA) in Sorensen's phosphate buffer pH 7.4 (Electron Microscopy Sciences). After several washes in buffer, heads were transferred into 1% osmium tetroxide (OsO_4) solution (Electron Microscopy Sciences) in distilled water for 1 h on ice followed by 1 h at 20°C. Tissue was washed several times in distilled water and finally treated with saturated ethyl gallate (1 h at 0°C and 1 h at 20°C). After staining, the heads were dehydrated, embedded in Ultra-Low Viscosity Embedding Media (Polysciences, Warrington, PA, USA) and serially sectioned at 8 μm. For SEM, whole animals were dried, mounted, gold-coated and viewed with a Philips SEM 505 microscope.

Experimental setup

After emergence, *X. peckii* males were anesthetized by cooling and tethered by their dorsal metathorax to a thin wire using Elmer's multi–purpose glue. All body parts were free to move, while the thorax remained in a fixed position at the center of a white cylinder (diameter 16 cm, height 18.5 cm). During experiments insects intermittently engaged in flight behavior, and frequently moved their legs. A computer-animated pattern of vertical black and white stripes was projected onto the inner surface of the cylinder using 'Vision egg' freeware (http://www.visionegg.org/) and a projector NEC VT 47 (NEC Corp., Tokyo, Japan) with a Mercury optics super wide 0.45× AF high definition digital lens with macro (Mercury Innovations, New York, NY, USA; see Fig. 2). Direct exposure of the insect to the projector light was prevented with a small disk of green paper. The pattern contrast was m=(I1–I2)/(I1+I2)=0.52, where I1 and I2 are light intensity values of the white and black stripes, respectively. Twelve different gratings, with spatial wavelengths of 10°, 15°, 18°, 20°, 24°, 30°, 36°, 45°, 60°, 72°, 90°, 120°, were rotated in the insects' yaw plane. The apparent width of the stripes decreases with the cosine of viewing elevation. At the upper and lower edges of the drum, which were each approximately 49° from the midline, apparent stripe width was 66% of that at eye-level. The insects' responses were recorded by a camera JAI CV S3200 (JAI A.S., Copenhagen, Denmark) with a Navitar zoom 7000 lens (Navitar Inc., Rochester, NY, USA) mounted above the cylinder. Angular velocity and spatial wavelength of the gratings co-varied so that their ratio, i.e. temporal frequency, was kept constant at 2 Hz, which is close to the optimum identified by Pix et al. for *Xenos vesparum* (Pix et al., 2000).

D. melanogaster males were tested in the same experimental setup, but with spatial wavelengths of 5°, 6°, 10°, 15°, 20° and 30°. It has been shown that *D. melanogaster* has its optimal response at temporal frequency of 1.3 Hz (Buchner, 1976). Thus, in our experiments with *Drosophila* temporal frequency was held constant at 1.3 Hz.

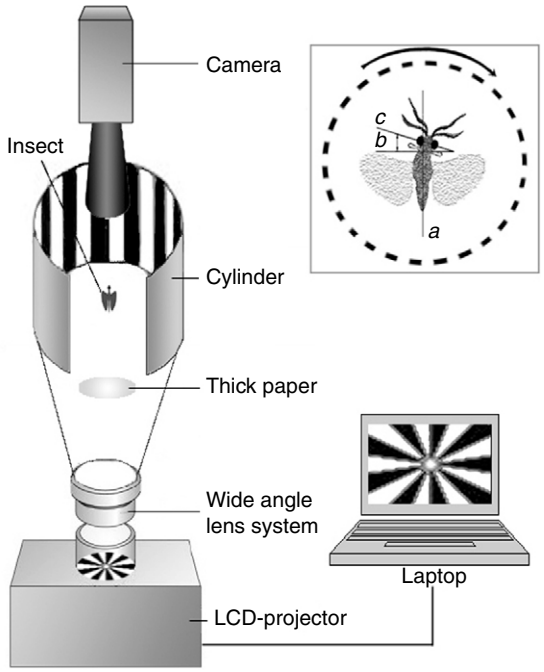

Fig. 2. Schematic of experimental setup. A computer generated stimulus was projected into a white cylinder, at the center of which an insect was mounted. Behavioral responses were recorded with a video camera for frame-by-frame analysis (inset). The animal's head deflection was measured as the angle between a line through the centers of both eyes [transverse axis of the head (*c*) and the transverse axis of the body (*b*)]. Longitudinal body axis (*a*) was used to determine the transverse axis of the body (*b*).

Quantifying the optomotor response

In both species the magnitude of head deflection was used to quantify the optomotor response; this was measured from video frames using 'ImageJ' software (NIH, Bethesda, MD, USA). Head deflection was defined as the angle between a line through the centers of both eyes (transverse axis of the head) and the transverse axis of the body (Fig. 2 inset). The eyes are the darkest part of the insects' anatomy, and so could be isolated as separate objects by thresholding the image; a line through the x, y coordinates of their centers was then used to compute angular deflections of the head on each frame. Head movements in the same direction as pattern rotation (clockwise or counter-clockwise) were designated positive, and those opposing the direction of the pattern were negative.

For each spatial wavelength, moving stimuli of 5 s duration were presented five times each in the clockwise and counter-clockwise directions. Direction alternated between successive presentations with 1.5 s intervals of no stimulation. The onset phase of the response lasted less than 2 s, and so head deflection measurements are taken from the last 3 s – the equilibrium phase – of each trial. Head deflection was determined for every third frame (i.e. 10 f.p.s.), resulting in 30 measurements for each of 10 trials (5 times for each direction), giving 300 measurements per individual per spatial wavelength. The mean of these 300 measurements, combining clockwise and counter-clockwise responses, was recorded as the magnitude of the response to a given spatial wavelength.

EMD model

Head deflection magnitudes were modeled as the output of correlation-type elementary movement detectors (EMDs) using Eqn 1 (Pix et al., 2000). When stimulated with a sinusoidal grating the equilibrium phase of the response (R) is a function of the angular velocity (ν) and the spatial wavelength (λ) of the stimulus and three variables: time constant (τ), the angular separation between input elements (the sampling base $\Delta\Phi$), and half-width of the angular sensitivity function of the input elements (the acceptance angle $\Delta\rho$):

$$R = \frac{1}{\sqrt{1 + (2\pi\tau\nu/\lambda)^2}} \sin[\arctan(2\pi\tau\nu/\lambda)] \times \sin(2\pi\Delta\phi/\lambda) \frac{1}{\sqrt{1 + (\Delta\rho/\lambda)^2}}. \quad (1)$$

Here we summarize the details of Eqn 1, previously described by Pix et al. (Pix et al., 2000). The response of the model depends on the temporal frequency ω of the stimulus, the ratio of the stimulus velocity and spatial frequency ($\omega=\nu/\lambda$). Therefore temporal frequency was held constant throughout the experiments. The first term in Eqn 1, $1/\sqrt{1+(2\pi\tau\nu/\lambda)^2}$, is the amplitude factor of the first order low-pass filter in the EMD. The second term, $\sin[\arctan(2\pi\tau\nu/\lambda)]$, sets the EMD to an optimal temporal frequency.

The third, so-called 'interference term', $\sin(2\pi\Delta\phi/\lambda)$, modulates the response based on the relation between the spatial pattern properties and of the detector sampling base. The sampling base $\Delta\Phi$ is the angular separation between input elements, and represents the most important parameter in our investigation. In biological visual systems the sampling base can be the angular spacing between individual photoreceptors, groups of photoreceptors or ommatidial units, and it determines the spatial resolution of the motion detection system (Borst and Egelhaaf, 1989). The smallest spatial wavelength λ that can be resolved by any visual system is equal to $2\Delta\Phi$ (Shannon and Weaver, 1949). For spatial wavelengths less than $2\Delta\Phi$ ($\Delta\Phi<\lambda<2\Delta\Phi$), moving stimuli appear to move opposite the direction of their actual motion, and the optomotor response occurs in the direction opposite that of the stimulus, due to aliasing (Götz, 1964). In this way the spatial wavelength at which the optomotor response changes from moving with, to moving against, the direction of the stimulus rotation indicates the spatial resolution of the motion detection system.

The last term, $1/\sqrt{1+(\Delta\rho/\lambda)^2}$, modulates the response as a spatial low-pass filter, depending on the relation between the acceptance angle $\Delta\rho$ and the stimulus spatial frequency $1/\lambda$. Photoreceptor spatial sensitivity distribution can be approximated with a Gaussian curve and the width of this curve at half its greatest magnitude is the acceptance angle ($\Delta\rho$) (Snyder, 1979; Smakman et al., 1984). Photoreceptors spatially integrate the luminance distribution within their visual field, acting as spatial low-pass filters. As a consequence, only low spatial frequencies ($1/\lambda \ll 1/\Delta\rho$) pass through the optics of the visual system with near-full contrast, and contrast at frequencies approaching $1/\Delta\rho$ is highly attenuated (Buchner, 1976; Land and Nilsson, 2002). Therefore, the size of the acceptance angle sets the cut-off frequency ($1/\Delta\rho$) of the visual system, which is the highest spatial frequency that can be transmitted through the optics with some detectable contrast present in the image.

Since the model output is dimensionless, we have expressed both the empirical and model response amplitudes as a fraction of the maximum response. It was not necessary to define the time constant τ, because after normalization the curves do not depend on the value of τ, which needs only to be non-zero. It should be noted that Eqn 1 was actually developed to predict the response of an EMD to sinusoidal intensity gratings. However, in our study we used square-wave gratings. It is not clear what effect is brought about by the additional harmonics in the square wave, but we suspect it is minor, based on how well our model matches the predictable behavior of *Drosophila* (see Results section).

Eqn 1 models EMDs with a single sampling base, but as stated in the introduction we hypothesize that in *X. peckii* there are two sampling bases, and so our model sums the output of two principal EMDs. Furthermore, due to variability in the geometry of the array, some pairs of receptor neighbors – input elements to the EMD – would be successively stimulated by the moving edges with a shorter interval than other pairs, and so a range of different effective sampling bases could be reflected in the optomotor behavior. Therefore, as in the model of Pix et al. (Pix et al., 2000), the two principal sampling bases in our model each have variability around a mean: they were the weighted sums of at least three small and three large sampling bases, both assumed to be normally distributed and equally spaced within the intervals $\bar{\chi}_{\Delta\Phi_1}\pm1$s.d.$_1$ (for the small base) and $\bar{\chi}_{\Delta\Phi_2}\pm1$s.d.$_2$ (for the large base), and weighted according to their respective normal distributions. The standard deviations (s.d.) were always less than half of the mean sampling base. Initial optimization was done with three small and three large sampling bases, and the number of bases was increased until the value being

optimized (the summed absolute difference between model and data) fell below an arbitrarily small threshold. After summation within the two principal bases, the smaller one was weighted with bias B, to allow for the possibility of a stronger contribution from one of the bases as in *Drosophila* (Buchner, 1976), and the two were summed and normalized to give the final output.

The values of $\Delta\Phi$ and their standard deviations, $\Delta\rho$ and the bias term B, were optimized with Matlab's *fminsearch* function (The Mathworks, Natick, MA, USA) to produce the best fit between the model and the empirical measurements of the insects' optomotor response. Due to trapping by local minima, optimization algorithms may produce different results from different initial parameters ('trapping effect').

Thus, we ran the above optimization 1000 times, with initial values drawn from uniform random distributions having the following overlapping ranges: $\overline{\chi}_{\Delta\Phi_1}$=1–27°, $\overline{\chi}_{\Delta\Phi_2}$=13–40° and $\Delta\rho$=3–25° (for *Strepsiptera*), and $\overline{\chi}_{\Delta\Phi_1}$=1–10°, $\overline{\chi}_{\Delta\Phi_2}$=5–15° and $\Delta\rho$=0.1–10° (for *Drosophila*). In both cases initial s.d.$_1$ and s.d.$_2$ were one-half the initial sampling bases, and B was between 0.5–3.0. In this way we objectively optimized the six relevant parameters: mean small and large sampling bases ($\overline{\chi}_{\Delta\Phi_1}$ and $\overline{\chi}_{\Delta\Phi_2}$), their standard deviations (s.d.$_1$ and s.d.$_2$), a bias (B), and acceptance angle ($\Delta\rho$).

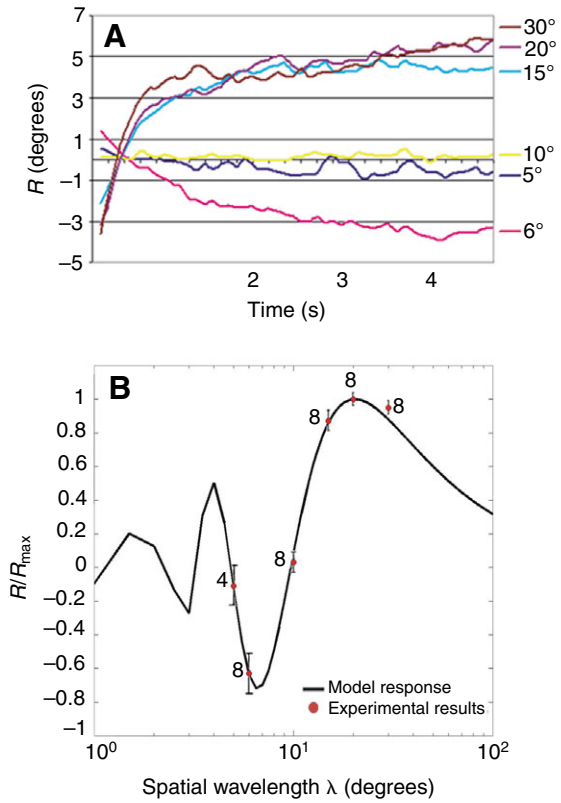

Fig. 3. *Drosophila* optomotor behavior. (A) Average response of eight (except for 5°, where N=4) individuals to six different spatial wavelengths. Positive values indicate head deflections with the direction of the pattern, and negative values indicate deflections in the reverse direction. (B) For each wavelength the cumulative, normalized, mean of the last 3 s is indicated by a circle ± s.e.m. bars. The solid line is the best-fitting EMD model, with mean sampling bases of 4.8° and 4.9° with s.d. of 0.1° for both, acceptance angle of 7°, and a bias B of 1.02 towards the smaller sampling base. Numbers indicate sample sizes for each spatial wavelength.

Results

Since the functional characteristics of the *Drosophila* visual system have been known for a long time, we used it to test the

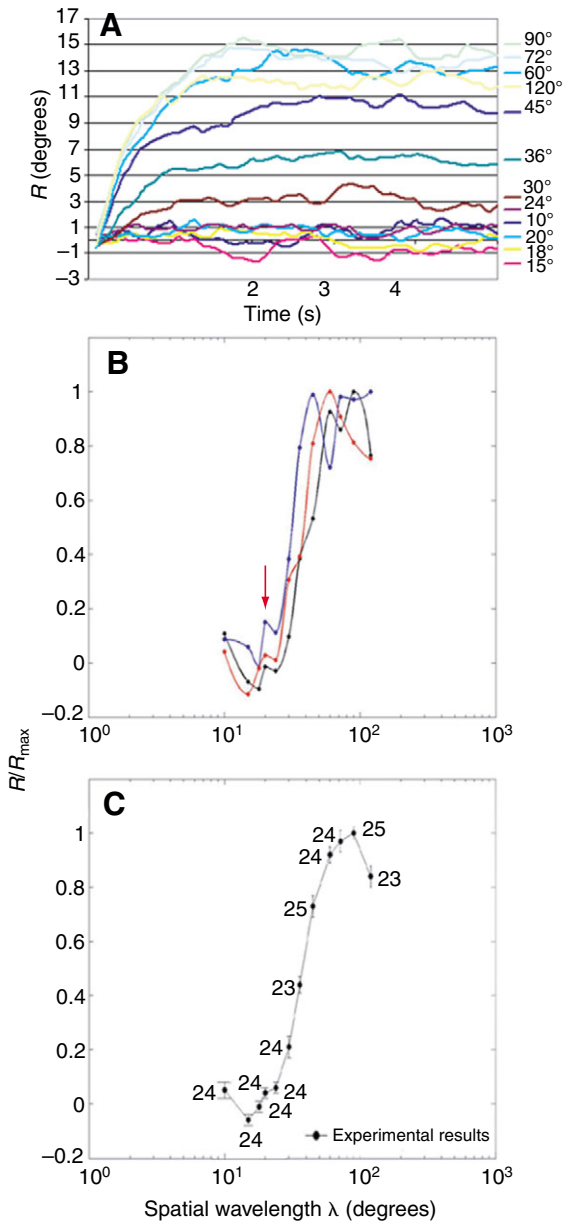

Fig. 4. *Xenos peckii* optomotor behavior. (A) Average responses of all tested individuals to 12 different spatial wavelengths. As in Fig. 3, positive values indicate head movements following the direction of the pattern, and negative values indicate head movements in reverse direction. (B) Examples of three normalized, average responses of the last 3 s to each wavelength. Although details of the curves vary, each of them is characterized by a local maximum between 18° and 24° (arrow). (C) For each wavelength the cumulative normalized response of the last 3 s of all individuals is indicated by a circle ± s.e.m. The number of individuals that were tested for each of the points are indicated.

validity of our experimental protocol and EMD model. Fig. 3A shows optomotor responses of *D. melanogaster* evoked by six spatial wavelengths. Head rotations with the direction of the pattern are clearly visible for spatial wavelengths of 15°, 20° and 30°, and a negative response indicates aliasing at a spatial wavelength of 6°. Responses to spatial wavelengths of 5° and 10° are very weak, barely deviating from 0° for the entire 5 s stimulation. Note that at the onset of each response the head was generally turned in the opposite direction, still somewhat locked into position from the previous stimulus presentation. The length of the onset phase (the time period that precedes a stable response) varies somewhat for different spatial wavelengths but generally lasts less than 2 s, so only the last 3 s were used for analysis.

In Fig. 3B mean responses are plotted together with standard errors of the mean (s.e.m.). The maximum response occurs at λ=20°, where mean head deflection reaches about 5°. As mentioned above, at a spatial wavelength of 10° hardly any response is observed, and at 6° the response is strongly opposed to the direction of the stimulus, meaning the largest wavelength to produce aliasing, which should equal 2ΔΦ, is close to 10°. As with Strepsiptera, the optimization of the model had two principal sample bases. However, in the best fit for our experimental data (Fig. 3B black curve) the two sample bases converged toward nearly identical values. Each principal base was composed of the three bases with means of 4.8° and 4.9°, s.d. of 0.1° for both of them, a bias of 1.02, and an acceptance angle of 7°. These are in good agreement with reported values for ΔΦ in *D. melanogaster* (around 5°) (Buchner, 1976; Land and Nilsson, 2002) and Δρ (varies between 3.5° and 7° with adaptation state) (Buchner, 1976). We were therefore confident that our behavioral protocol and model could be profitably applied to the Strepsiptera motion detection system. We note that the repeated optimization did not always produce these values, which is an important point that will be addressed in the Discussion.

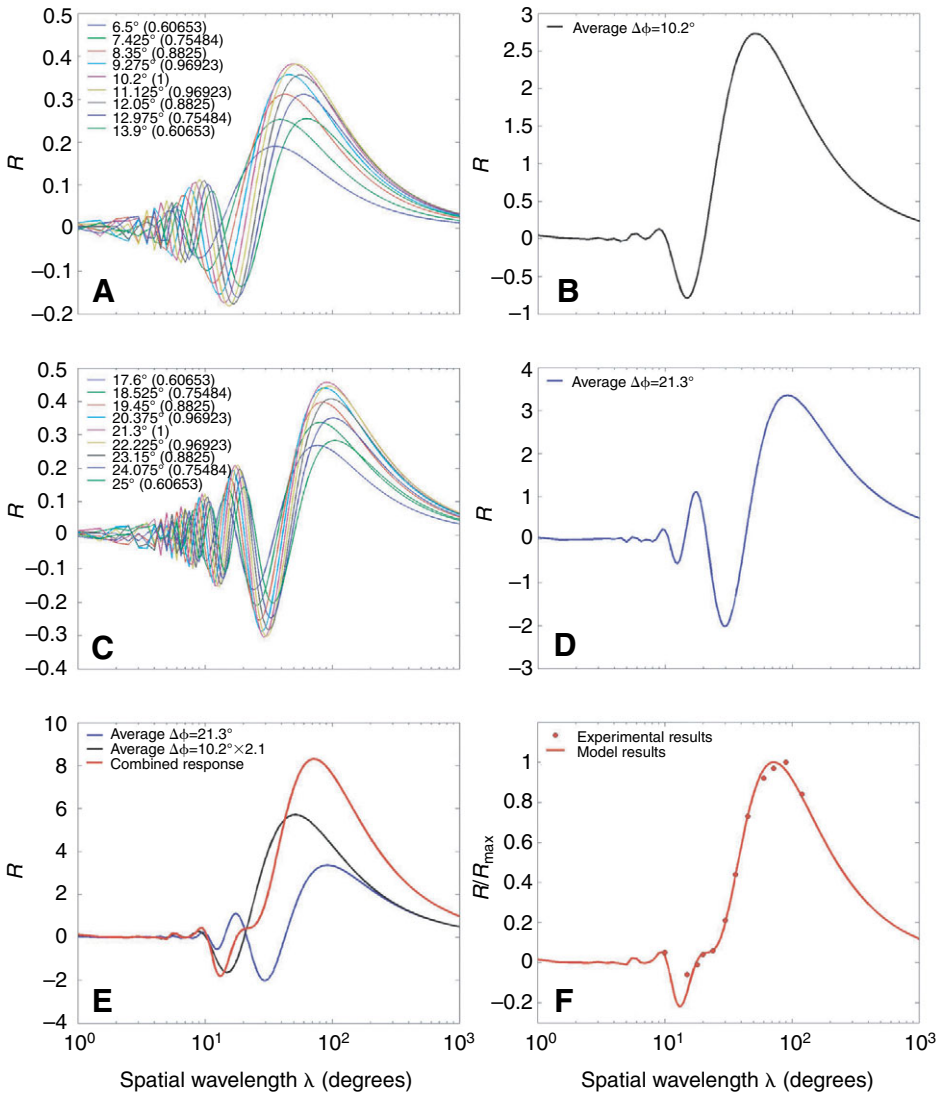

Fig. 5. The EMD model for *Xenos peckii*. (A) Nine small sample bases were calculated and summed into a single curve (B), which would be the response curve if only the smaller principal sample base and its variation were present. (C) Similarly nine larger sample bases were calculated and summed into the curve in (D). Numbers enclosed in parentheses in A and C indicate weights for respective sampling bases. (E) For the final model output the two curves illustrated in B and D were summed after multiplying the smaller sampling base response by the bias value (2.1). (F) The normalized version of the model response (solid line) is used to illustrate the close fit of experimental data (circles).

The general shapes of *X. peckii* responses to 12 spatial wavelengths are comparable to those of *Drosophila* (Fig. 4A). As in *Drosophila*, the length of the onset phase varied with the spatial wavelength, but was concluded in less than 2 s. A negative response indicating spatial aliasing, although not as strong as in *Drosophila*, is evident at 15°. Close examination of the responses of three different animals reveals a feature that will prove important for our analysis: although the details of the curves vary somewhat, each is characterized by a small, local maximum around 18–24° (Fig. 4B, arrow). This feature is present in all individuals for which these wavelengths were measured. The pooled responses of 23–25 animals show a maximum at a spatial wavelength of 90°, at which head deflection was more than 10°, and a reversal in the direction of head rotation at a wavelength of 15° (Fig. 4C). The small plateau between 18° and 24° is where individual local maxima have nearly been averaged out. We believe that the presence of these local maxima around 20° indicates that the strepsipteran optomotor response is based on one small and one large principal sampling base (see below).

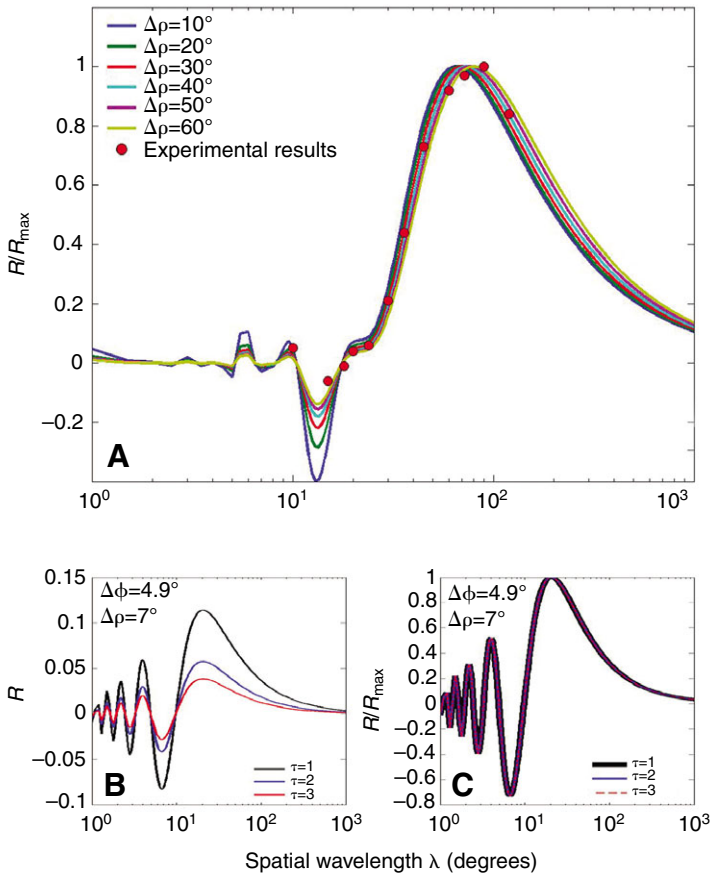

Fig. 6. The EMD model for *Xenos peckii* is relatively insensitive to the acceptance angle (Δρ) and independent of the time constant (τ). (A) Response curves between Δρ 10° and 60° result in similar fits of the experimental data, except for the degree of aliasing, which is strongest for the smallest values. (B) Eqn 1 is used to illustrate that the time constant (τ) affects only the amplitude of the calculated response. Three different time constants result in curves with different amplitudes. However, results are independent of τ, as curves are normalized to the maximum response (C).

The model output that best fit our empirical data resulted in nine sampling bases with a mean of 10.2°, nine with a mean of 21.3°, s.d. of 3.7° for both, bias of 2.1 and an acceptance angle of 37° (Fig. 5A,C). To illustrate the modeling procedure, these nine individual responses for the small and large sampling bases were weighted according to their respective normal distributions, and summed to give one curve for small and one for large principle sampling base (Fig. 5B,D). Curves like these would be expected if motion detectors integrated only a small or large sampling base (with variability), respectively. The small sampling base curve was weighted by B, and the two curves were summed to give the final model output (Fig. 5E). For comparison with the behavioral data, the model response amplitude (R) was normalized to the maximum response (R_{max}) (Fig. 5F).

It is noteworthy that although the EMD model was based on several variables, the outcome was only truly sensitive to changes in sampling base. Large changes in acceptance angle produced only minor shifts in the response peak (Fig. 6A), only really affecting the amplitude of the negative (aliasing) response. As the acceptance angle increased the amplitude of the negative response of the curve decreased. The time constant τ had no effect on the final outcome, because it only affects the amplitude of the EMD response. Fig. 6B illustrates three responses that had different amplitudes as a result of three different time constants, but this effect was eliminated after the responses were normalized (Fig. 6C). The overall fit of the model was also relatively insensitive to the bias. However, only a bias around 2 closely fit the critical wavelength between 18° and 24°.

Discussion

The optomotor response of *Xenos peckii* was best fit by an EMD model that combined two distinctly different sampling bases: one of approximately 10° and the other around 21°. As evidence for this, we show that the specific shape of the behavioral response curve, particularly the local maximum around a spatial wavelength of 20°, cannot be fit with a motion detection model with one principal sampling base (see Fig. 3B, Fig. 5A–D). This notion is further supported by the 1000 pseudo-randomized optimizations. A histogram shows that the most common outcome for *X. peckii* was one base around 10–13° and one around 20–22° (Fig. 7A,B). The smaller peaks near 20° in Fig. 7A and near 10° in Fig. 7B resulted from the optimization process reversing the two bases, because of the overlapping ranges of initial states. The rare instances (~50) in which both bases occurred in one of these peaks were characterized by poor fits to the data. This result for *X. peckii* was corroborated by the identical process carried out on *Drosophila*. The most common outcome in this case was a base at 5°, and a second base at either 10° or 15° (Fig. 7C,D); all peaks are predictably sharper than those for *X. peckii*. While it may appear that the larger sampling bases in both *X. peckii* and *Drosophila* were harmonic artifacts of the smallest base (after all, the stimulus and model were based on sinusoids), this cannot be the case – there are no peaks above 20–22° for *X. peckii* nor above 15° for *Drosophila*. Indeed, the outcome for *Drosophila* is well-supported by Buchner's (Buchner, 1976) finding that pairs of EMD input elements may span one or even two rows of ommatidia, and in fact our results support one of Buchner's two candidate models for how this is done [fig. 11C in Buchner (Buchner, 1976)].

We think that the presence of two sampling bases may have resulted from integrating simple eyes into the framework of a compound eye. While the geometry and results clearly point to a smaller sampling base within individual camera-type eyelets, the composition of the larger sampling base is less straightforward. It may be based on pairs of input elements from different eyelets, pairs of EMD input elements that skip nearest neighbors within single eyelets, or a combination of both. In the following section we present two alternative possibilities for how the large sampling base could result from input elements of different eyelets.

The first possibility is that EMDs are situated between each sampling unit of one eyelet and its corresponding sampling unit in the neighboring eyelet, as illustrated in Fig. 8B. The average larger sampling base in *X. peckii* around 21° (Fig. 7B) is

narrower than the average anatomical separation between two neighboring eyelets, around 27° (Buschbeck et al., 2003). This disparity may have to do with the relationship between inter-receptor angle and sampling base. Compound eyes typically are composed of a hexagonal array of facets. Depending on the orientation of the array, the effective horizontal sampling base does not correspond to the angle between neighboring ommatidia, but to $\sqrt{3}/2$ or 1/2 of that value (Fig. 8A). The sampling base of *X. vesparum* was estimated to be 9°, or precisely one-half the anatomical inter-eyelet separation of 18° (Pix et al., 2000). This is consistent with a hexagonal array in the 'standing' orientation. The large sampling base of *X. peckii*, on the other hand, is more consistent with an array in the 'lying' orientation, i.e. $(27\cdot\sqrt{3})/2=23.4°$. If this angle is twice the smaller (intra-eyelet) base, EMDs composed of all corresponding visual units in neighboring eyelets would give a larger sampling base close to what we observe (Fig. 8B). Because eyelets are arranged irregularly, some groups of neighboring eyelets are more or less hexagonally arranged, whether standing or lying, but many are not (Fig. 8C). Given this mixed geometry it is not surprising that the apparent sampling base does not exactly match the standing or lying array (see Fig. 7B, Fig. 8A), the precision found in *X. vesparum* notwithstanding. This geometrically simple and elegant solution could have evolved if single ommatidia in the ancestral compound eye turned into eyelets by increasing the number of receptor cells. The neuroanatomical implication of such an organization is that extensive collateral projections within the optic lobes would be necessary to accommodate anatomically distant input channels.

The alternative possibility is that inter-eyelet EMDs are only present near the edges of neighboring eyelets. In this scenario only those units of adjacent eyelets that sample neighboring visual fields would be connected. This can be best illustrated schematically on a histological section, such as in Fig. 8D. In this example, the third eyelet from the left is sectioned through its periphery. Here only a small piece of retina is visible, which could correspond to a single sampling unit. Within this horizontal section, the next eyelet to the right is slightly off axis as well, perhaps allowing for the presence of three neighboring sampling units. In this plane, the angle between the optically nearest sampling units of these two eyelets then would be 23° (Fig. 8D). The angle between the optically nearest sampling units between the fourth and fifth eyelet would be 18°. The large sampling base in this scenario results from the average of such connections. This solution is geometrically complex and it is difficult to gauge specifically how sampling bases are distributed. However, this is the organization that would require fewest modifications within neuropils, and could have evolved through the coalescence of clusters of ancestral omatidia. At the neuroanatomical level inhomogeneities are expected, but no extensive collateral projections would be required. Future anatomical investigations could provide evidence for either of the two scenarios.

Considering that motion detection within eyelets theoretically could have evolved *de novo*, it is possible that it could follow a mechanism other than the correlation EMD model that otherwise is widely accepted in insects. Specifically, motion detection might operate by the gradient model proposed by Srinivasan (Srinivasan and Zhang, 1997) to explain how honey bees use image speed to center their flight path within a tunnel, even though correlation models best explain their optomotor behavior (Srinivasan et al., 1993). Buchner (Buchner, 1984) showed that gradient models are expected to result in very different response curves from those of correlation models, if the temporal frequency is held constant over a range of special wavelengths [compare fig. 11c and g in Buchner (Buchner, 1984)]. Based on our experimental results, which generally follow the sinusoidal shape of correlation type motion detectors, it seems likely that both intra- and inter-eyelet EMDs are based on correlation-type motion detection. However, without detailed modeling, it is difficult to predict what the response would be if the two motion detection mechanisms were combined. Concerning our findings, it is noteworthy that, according to Buchner

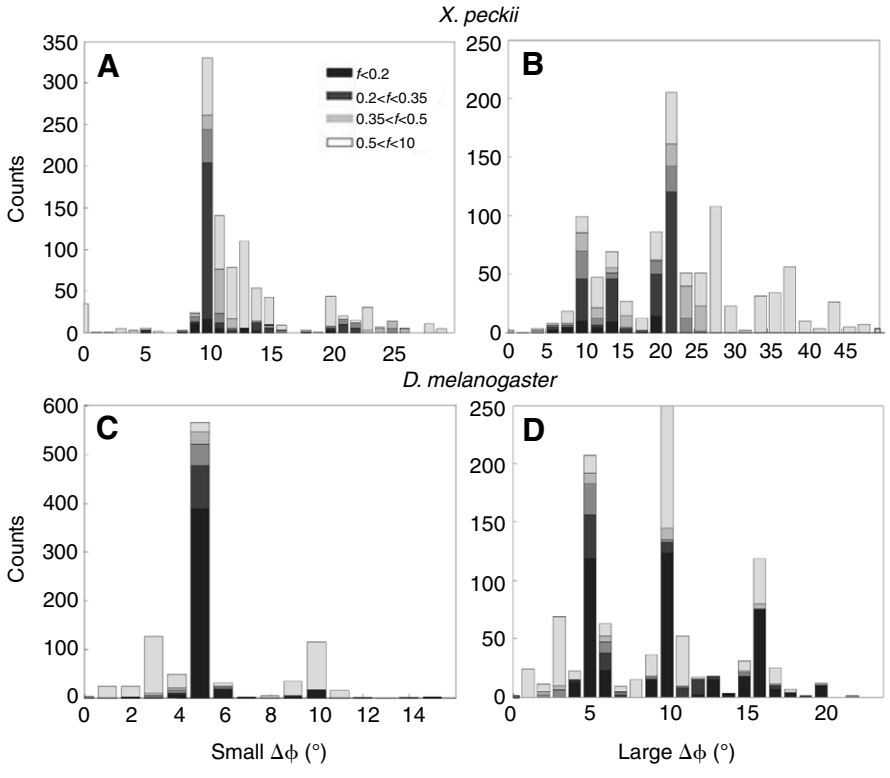

Fig. 7. Sampling bases resulting from 1000 optimizations. Initial states were drawn from uniform random distributions between $\bar{\chi}_{\Delta\Phi_1}$=1–27°, $\bar{\chi}_{\Delta\Phi_2}$=13–40° and $\Delta\rho$=3–25° for *X. peckii* (A,B), and between $\bar{\chi}_{\Delta\Phi_1}$=1–10°, $\bar{\chi}_{\Delta\Phi_2}$=5–15° and $\Delta\rho$=0.1–10° for *Drosophila* (C,D). In both cases s.d.$_1$ and s.d.$_2$ were one-half the initial sampling bases. Gray scale is proportional to *f*, the sum of the absolute difference between empirical data and model, darkest bars indicating best fit (see key in A).

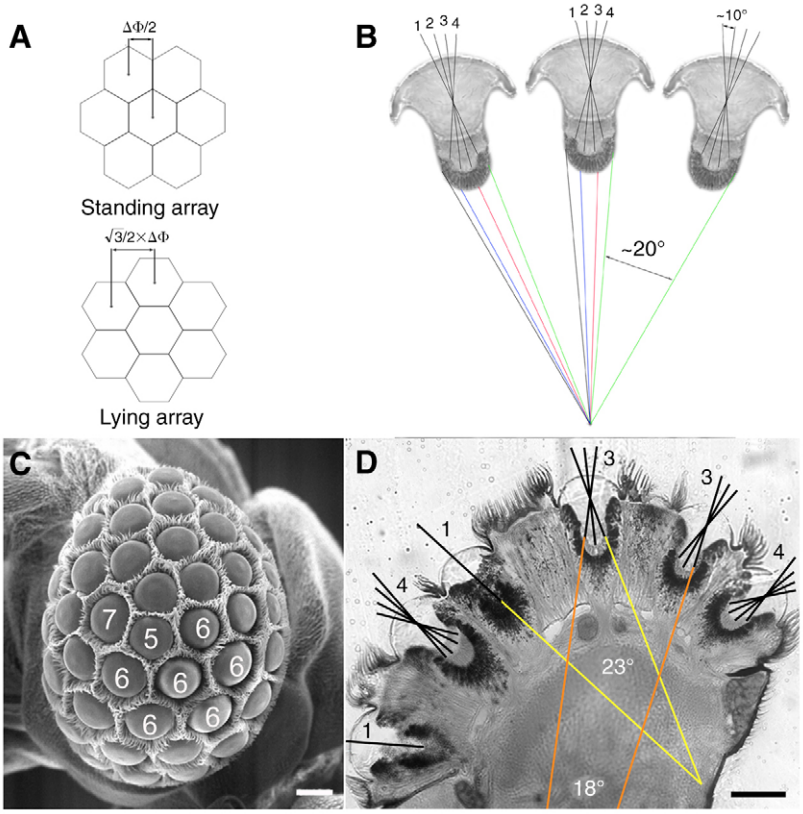

Fig. 8. Geometrical interpretations of sample bases. (A) Geometry of standing and lying hexagonal arrays. (B) Hypothetical organization of sampling units in three neighboring eyelets. The retina of one eyelet has up to four sampling units in the horizontal plane, subsuming a total of about 30–35°. The smaller sampling base around 10° occurs within an eyelet, for instance between units 1–2, 2–3, 3–4 in the middle eyelet. One possibility for the larger sample base around 20° is that neighboring eyelets span, for instance between units 1–1, 2–2, etc. (C) Irregularities in the organization of eyelets indicated by the number of nearest neighbors for several specific eyelets. (D) A horizontal section of *X. peckii* illustrates an alternative explanation for the larger sample base, connecting only nearest optical neighbors. The angles of two such connections are indicated. Variation results because some eyelets lie in the same horizontal plane as their neighbors, such as those in which the same number of sampling units are visible (their optical axes in 2D indicated with straight lines), while other neighbors lie outside the horizontal plane, such as those in which different numbers of units are visible. Scale bars, 50 μm.

(Buchner, 1984), both models predict identical zero crossings, and so either model would support processing within eyelets.

Our estimated acceptance angle of 37° is relatively large compared to other insects (Land, 1997). Previous measurements of *X. peckii* eyes show that the angular width of a whole eyelet retina (projected through the nodal point of the lens) is about 33° (Buschbeck et al., 2003). Considering our current results, however, it is unlikely that the whole retina acts as an input element. The EMD model is relatively insensitive to the magnitude of the acceptance angle (see Fig. 6A) – the s.d. of 1000 optimized values was 36° – and this should be verified using more direct means.

There are important differences between the results for *X. peckii* and those for *X. vesparum*. The latter did not exhibit the reversed optomotor turning that indicates spatial aliasing, and Pix et al. (Pix et al., 2000) attribute this primarily to an irregular sampling array. Indeed, the reversal in turning direction is lost even in a very regular lens array like that of *Drosophila* when the stimulus grating is not aligned perpendicular to the principal EMD orientation (Buchner, 1976); such misalignment is surely the case over much of the strepsipteran eye, and so this conclusion is reasonable. Also, *X. vesparum* did not produce a local response maximum at ~20°. While these differences in performance may indicate different motion-detection systems, alternative explanations include the difference in wavelength intervals tested in the critical region, the larger eyelets of *X. pekii* with their greater number of receptor cells, the difference in sample sizes (the smallest being 23 rather than 3) and, most importantly, the fact that our model was predicated on two distinct sampling bases rather than one.

Based on our results, we propose that at its widest extent the retina of one eyelet has four sampling units in the horizontal plane (four sampling units separated by 10° gives a total extent of 30°; see Fig. 8B). Assuming a symmetrical, round retina, one eyelet can have up to 13 points of resolution (based on πr^2). This value falls well within the 6–35 points previously estimated from histological sections (Buschbeck et al., 2003). Since each eyelet has around 100 receptor cells (Buschbeck et al., 2003), and each EMD input element is formed by approximately eight receptor cells. This is an intriguing parallel with the ommatidia of typical compound eyes, in which the signals from 8–10 photoreceptors are also pooled, and even with the neural superposition compound eyes of flies such as *Drosophila*, in which eight photoreceptors from seven different ommatidia sample each point in space. Since an abundance of photoreceptor cells is costly (Laughlin et al., 1998) it may be that natural selection produces the minimum number of receptors necessary to adequately sample each point in the visual field; if this is the case, in compound eyes the minimum number is approximately eight. Since vision has several modalities (detection of color, brightness, motion, etc.) and the optomotor response is exclusively based on motion detection, our conclusions refer to the motion detection system specifically. It is possible that some of the photoreceptors primarily serve other visual tasks, possibly even utilizing visual pathways with different spatial resolution.

We thank Sarah Sbita for technical assistance, Irena Nikcevic and Ilya Vilinsky for helpful discussions and Nadine Stecher for comments on the manuscript. This work has been supported by a Wieman-Wendell fellowship to S.M. and by the NSF (IBN-0423963 and IOB-0545978).

References

Borst, A. and Egelhaaf, M. (1989). Principles of motion detection. *Trends Neurosci*. **12**, 297-306.

Borst, A. and Egelhaaf, M. (1993). Detecting visual motion: theory and models. In *Visual Motion and its Role in the Stabilization of Gaze* (ed. F. A. Miles and J. Wallman), pp. 3-27. Amsterdam, London: Elsevier.

Buchner, E. (1976). Elementary movement detectors in an insect visual system. *Biol. Cybern.* **24**, 85-101.

Buchner, E. (1984). Behavioural analysis of spatial vision in insects. In *Photoreception and Vision in Invertebrates* (ed. M. A. Ali), pp. 561-621. New York: Plenum.

Buschbeck, E. K., Ehmer, B. and Hoy, R. R. (1999). Chunk versus point sampling: visual imaging in a small insect. *Science* **286**, 1178-1180.

Buschbeck, E. K., Ehmer, B. and Hoy, R. R. (2003). The unusual visual system of the Strepsiptera: external eye and neuropils. *J. Comp. Physiol. A* **189**, 617-630.

Egelhaaf, M. and Borst, A. (1993). Movement detection in arthropods. In *Visual Motion and its Role in the Stabilization of Gaze* (ed. F. A. Miles and J. Wallman), pp. 53-77. Amsterdam, London: Elsevier.

Götz, K. G. (1964). Optomotorische Untersuchungen des visuellen Systems einiger Augenmutanten der Fruchtfliege *Drosophila*. *Kybernetik* **2**, 77-92.

Hughes, D. P., Beani, L., Turillazzi, S. and Kathirithamby, J. (2003). Prevalence of the parasite Strepsiptera in *Polistes* as detected by dissection of immatures. *Insectes Soc.* **50**, 62-68.

Johnston, J. S., Ross, L. D., Beani, L., Hughes, D. P. and Kathirithamby, J. (2004). Tiny genomes and endoreduplication in Strepsiptera. *Insect Mol. Biol.* **13**, 581-585.

Kinzelbach, R. (1967). Zur Kopfmorphologie der Fächerflügler (Strepsiptera, Insecta). *Zool. Jb. Anat.* **84**, 559-684.

Kinzelbach, R. K. (1971). Morphologische Befunde an Fächerflüglern und ihre phylogenetische Bedeutung (Insecta: Strepsiptera). *Zoologica* **41**, 1-256.

Kritsky, G., Wells, D. G. and Mari Mutt, J. A. (1977). Some observations on the fine-structure morphology of *Xenos peckii* (Coleoptera: Stylopidae). *Coleopt. Bull.* **31**, 93-96.

Land, M. F. (1997). Visual acuity in insects. *Annu. Rev. Entomol.* **42**, 147-177.

Land, M. F. (1999). Motion and vision: why animals move their eyes. *J. Exp. Biol.* **185**, 341-352.

Land, M. F. and Nilsson, D.-E. (2002). *Animal Eyes*. Oxford: Oxford University Press.

MacCarthy, H. R. (1991). Compound eye of male *Stylops pacifica* (Strepsiptera; Stylopidae). *J. Entomol. Soc. Brit. Columbia* **88**, 27-31.

Laughlin, S. B., van Steveninck, R. R. D. and Anderson, J. C. (1998). The metabolic cost of neural information. *Nat. Neurosci.* **1**, 36-41.

Nilsson, D.-E. (1989). Optics and evolution of compound eyes. In *Facets of Vision* (ed. D. G. Stavenga and R. C. Hardie), pp. 30-73. Berlin: Springer.

Paulus, H. F. (1979). Eye structure and the monophyly of the Arthropoda. In *Arthropod Phylogeny* (ed. A. P. Gupta), pp. 299-384. New York: Van Nostrad Reinhold.

Pix, W., Zanker, J. M. and Zeil, J. (2000). The optomotor response and spatial resolution of the visual system in male *Xenos vesparum* (Strepsiptera). *J. Exp. Biol.* **203**, 3397-3409.

Proffitt, F. (2005). Twisted parasites from 'Outer Space' perplex biologists. *Science* **307**, 343.

Rösch, P. (1913). Beiträge zur Kenntnis der Entwicklungsgeschichte der Strepsipteren. *Z. Naturw.* **50**, 97-146.

Shannon, C. E. and Weaver, W. (1949). *The Mathematical Theory of Communication*. Urbana: University of Illinois Press.

Smakman, J. G. J., van Hateren, J. H. and Stavenga, D. G. (1984). Angular sensitivity of blowfly photoreceptors: Intracellular measurements and wave-optical predictions. *J. Comp. Physiol. A* **155**, 239-247.

Snyder, A. W. (1979). Physics of vision in compound eyes. In *Handbook of Sensory Physiology*. Vol. VII/6A (ed. H. Autrum), pp. 225-313. Berlin, Heidelberg: Springer.

Srinivasan, M. V. and Zhang, S. W. (1997). Visual control of honeybee flight. In *Orientation and Communication in Arthropods* (ed. M. Lehrer), pp. 96-113. Basel: Birkhäuser Verlag.

Srinivasan, M. V., Zhang, S. W. and Chandrashekara, K. (1993). Evidence for 2 distinct movement-detecting mechanisms in insect vision. *Naturwissenschaften* **80**, 38-41.

Srinivasan, M. V., Poteser, M. and Kral, K. (1999). Motion detection in insect orientation and navigation. *Vis. Res.* **39**, 2749-2766.

Strausfeld, N. J. and Seyan, H. S. (1985). Convergence of visual, haltere, and prosternal inputs at neck motor neurons of *Calliphora erythrocephala*. *Cell Tissue Res.* **240**, 601-615.

Strohm, K. (1910). Die zusammengesetzten Augen der Männchen von *Xenos rossii*. *Zool. Anz.* **36**, 156-159.

Wachmann, E. (1972). Fine-structure of compound eye of Stylops spec. (Insecta, Strepsiptera). *Z. Zellforsch. Mikrosk. Anat.* **123**, 411-424.